



UNIVERSITY OF LEEDS

This is a repository copy of *A spheres-in-tube carbonaceous nanostructure for high-capacity and high-rate lithium–sulfur batteries*.

White Rose Research Online URL for this paper:
<http://eprints.whiterose.ac.uk/134468/>

Version: Accepted Version

Article:

Ge, Y, Chen, Z, Ye, S orcid.org/0000-0001-5152-5753 et al. (3 more authors) (2018) A spheres-in-tube carbonaceous nanostructure for high-capacity and high-rate lithium–sulfur batteries. *Journal of Materials Chemistry A*, 6 (30). pp. 14885-14893. ISSN 2050-7488

<https://doi.org/10.1039/C8TA05041D>

(c) The Royal Society of Chemistry 2018. This is an author produced version of a paper published in *Journal of Materials Chemistry A*. Uploaded in accordance with the publisher's self-archiving policy.

Reuse

Items deposited in White Rose Research Online are protected by copyright, with all rights reserved unless indicated otherwise. They may be downloaded and/or printed for private study, or other acts as permitted by national copyright laws. The publisher or other rights holders may allow further reproduction and re-use of the full text version. This is indicated by the licence information on the White Rose Research Online record for the item.

Takedown

If you consider content in White Rose Research Online to be in breach of UK law, please notify us by emailing eprints@whiterose.ac.uk including the URL of the record and the reason for the withdrawal request.



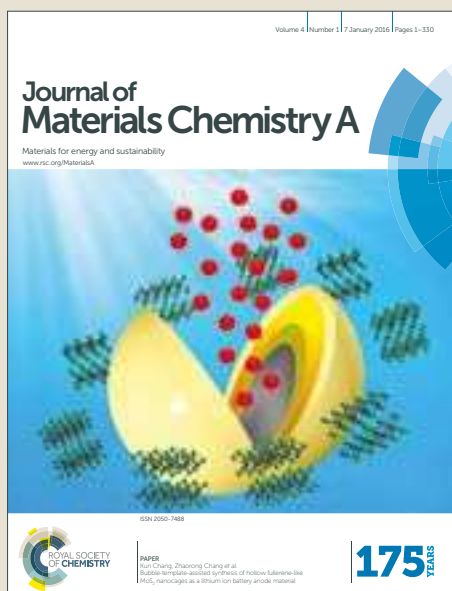
eprints@whiterose.ac.uk
<https://eprints.whiterose.ac.uk/>

Journal of Materials Chemistry A

Accepted Manuscript



This article can be cited before page numbers have been issued, to do this please use: X. Yang, Z. Chen, Z. Zhu, Y. Ge, S. Ye and Y. Tu, *J. Mater. Chem. A*, 2018, DOI: 10.1039/C8TA05041D.



This is an Accepted Manuscript, which has been through the Royal Society of Chemistry peer review process and has been accepted for publication.

Accepted Manuscripts are published online shortly after acceptance, before technical editing, formatting and proof reading. Using this free service, authors can make their results available to the community, in citable form, before we publish the edited article. We will replace this Accepted Manuscript with the edited and formatted Advance Article as soon as it is available.

You can find more information about Accepted Manuscripts in the [author guidelines](#).

Please note that technical editing may introduce minor changes to the text and/or graphics, which may alter content. The journal's standard [Terms & Conditions](#) and the ethical guidelines, outlined in our [author and reviewer resource centre](#), still apply. In no event shall the Royal Society of Chemistry be held responsible for any errors or omissions in this Accepted Manuscript or any consequences arising from the use of any information it contains.

A Spheres-in-Tube Carbonaceous Nanostructure for High-Capacity and High-Rate Lithium-Sulfur Batteries

Yuanhang Ge,^{a†} Ze Chen,^{a†} Sunjie Ye,^c Zhifeng Zhu,^a Yingfeng Tu,^a and Xiaoming Yang^{*ab}

Received 00th January 20xx,
Accepted 00th January 20xx

DOI: 10.1039/x0xx00000x

www.rsc.org/

The uses of sulfur, which although has a high theoretical specific capacity of 1675 mAh g⁻¹, as commercial cathode for lithium batteries have been substantially hindered by the insulating nature of sulfur and the dissolution of intermediate polysulfides (Li₂S_x, 4 < X ≤ 8) into the electrolyte. In this work, a spheres-in-tube carbonaceous nanoarchitecture has been successfully engineered as an effective sulfur host, by encapsulating heteroatom-doping hollow carbon spheres into an intact carbonaceous nanotube (I-HCSs@CT). The structural features including hierarchical porosity, intact nature of CT wall and HCS framework have cooperatively endowed I-HCSs@CT with outstanding capability of host loading, good electrical conductivity, high utilization rate and excellent stability of sulfur. As a result, our sulfur/carbon composites deliver a large discharge capacity of 1426 mAh g⁻¹ at 0.1 C with a high sulfur loading of 72.1 wt%. The obtained electrode demonstrates superior high-rate cycling performance, with a high specific capacity of 746 mAh g⁻¹ at 0.5 C retained after 500 cycles.

1. Introduction

High energy density is essential for next-generation rechargeable batteries to meet the increasing demand for electric vehicles and even grid-scale storage applications.¹ Lithium-sulfur (Li-S) batteries based on a multi-electron chemical reaction have been explored as a promising electrochemical energy storage system owing to their high energy density (~2500 Wh kg⁻¹), low cost, and environmental friendliness.² However, Li-S batteries still suffer from some critical problems that restrict their practical applications. First, the insulating nature of both sulfur and the reduction product of Li₂S limit the utilization of the active material and the rate performance of Li-S batteries.³ Secondly, the dissolution of polysulfide ions in an organic electrolyte causes reactions with the lithium anode, resulting in the so-called "shuttle effect".⁴ Thirdly, the large volumetric expansion (~80 %) of sulfur upon lithiation gives rise to electrode damage and cell degradation.⁵ As a consequence, Li-S batteries show poor cycling stability and low Coulombic efficiency.

To address these issues, a number of strategies have been developed to enhance the electric conductivity of sulfur and suppress the dissolution of polysulfide, including the use of electrically conductive hosts for sulfur,⁶ the insertion of interlayers,⁷

and the exploitation of new electrolytes/additives.^{8, 9} Carbon materials have been considered as excellent materials for sulfur host, because their high conductivity can improve the utilization rate of sulfur, and their large specific surface areas can lead the redox intermediates of sulfur to be effectively trapped.¹⁰ In particular, carbonaceous nanotubes (CTs) have been widely investigated as host materials in Li-S batteries, owing to their unique features of high charge transport capability, good electrolyte accessibility, large aspect ratio, good chemical stability, combined with large inner void space, which can greatly increase the sulfur loading and relieve the electrode volume change.¹¹⁻¹³ However, the electrochemical performance of CTs have been limited by their relative low specific surface area (SSA), poor porosity and low content of heteroatoms of CTs. More specifically, the capacity often decayed rapidly in the subsequent cycles because of the fluent pathway in CTs, and CTs-based sulfur host materials with low content of heteroatoms are nonpolar, hence less efficient in entrapping polar polysulfides.^{14,15} Therefore, it is of paramount importance to construct hybrid heteroatom-doped CTs-based materials that can be used as effective sulfur hosts to efficiently facilitate sulfur sorption, enhance conductivity of sulfur electrode and inhibit shuttle effect of polysulfides. The main strategies for creating such CTs-based host materials include: (1) utilizing the cavity of the nanotubes by inserting smaller active materials,¹⁶ (2) modifying the wall of CTs via coating a protective layer or designing gateways to hinder the penetration of polysulfides.¹⁷ For example, Wang and co-workers developed a tube-in-tube porous hollow carbon nanotube (small carbon nanotubes confined inside a large carbon nanotube), which can be used as a high-performance and high-rate flexible Li-S electrode.¹³ Lou and co-workers prepared CTs filled with MnO₂ nanosheets as efficient sulfur hosts, which not only facilitate electron and ion transfer during the redox reactions, but also efficiently avoid

^aState and Local Joint Engineering Laboratory for Novel Functional Polymeric Materials, Suzhou Key Laboratory of Macromolecular Design and Precision Synthesis, Jiangsu Key Laboratory of Advanced Functional Polymer Design and Application, Department of Polymer Science and Engineering, College of Chemistry, Chemical Engineering and Materials Science, Soochow University, Suzhou 215123, P. R. China. *E-mail: yangxiaoming@suda.edu.cn

^bKey Laboratory of Advanced Textile Materials and Manufacturing Technology, Ministry of Education.

^cSchool of Physics and Astronomy, University of Leeds, LS2 9JT, Leeds, UK.

†The two authors contribute equally to this work.

Electronic Supplementary Information (ESI) available. See DOI: 10.1039/x0xx00000x

polysulfide dissolution.¹⁶ Zhou and co-workers engineered permselective gateways for Li⁺ transportation in holey-CTs/S cathodes, which displayed improved ability of preventing Li-S intermediates penetration in energy storage application.¹⁷ These strategies have remarkably improved the energy storage ability of CTs/S composites, and provided implementations for further improvements: the inner cavity can be utilized more effectively, and the protective layer coating on the wall of CTs can be judiciously modified to enhance the electrolyte accessibility and block the mesopores on CTs surface.¹⁸⁻²⁰ To this end, it is imperative to design a simple and effective CTs-based structure, which not only strengthen the electrical conductivity and structural stability of sulfur electrode, but also provides high sulfur loading and utilization rate.

Herein, a novel spheres-in-tube structure with hollow carbon spheres encapsulated in an intact carbonaceous tube (I-HCSs@CT) was designed. Due to the high heteroatoms content, polypyrrole (PPy) was selected as carbon precursor and deposited on the surface of the channels of anodic aluminum oxide (AAO). SiO₂ NPs were subjected to the confined assembly to be encapsulated in the PPy tube channel. The as-obtained SiO₂@PPy@AAO template was coated by PPy again, followed by carbonization and template removal to form I-HCSs@CT. Numerous HCSs are grown inside a CT, which can significantly improve the electrical contact, mitigate the internal shuttling effect and buffer the volume change of sulfur cathodes. Consequently, the I-HCSs@CT/S composites exhibit a large reversible capacity, excellent rate performance and good cycling stability.

2. Experimental Section

2.1 Chemicals

Anodic aluminum oxide (AAO) membranes with pore size of 200 ± 16.7 nm were purchased from Puyuan Nanotech, Co., Ltd., China. These membranes are freestanding disks with a diameter of 25 mm and a thickness of 60 μm, with double-pass channels. Pyrrole (Aldrich, 99%) is used after distillation under reduced pressure and stored under argon atmosphere at 4 °C. Ultrapure water (18.2 MΩ·cm⁻¹) was used directly from Milli-Q water system. Tetra-ethyl-orthosilicate (TEOS, A.R.), ammonia hydroxide (NH₄OH, 28%, A.R.), anhydrous ferric chloride (FeCl₃, 98%), hydrofluoric acid (HF, A.R.), Sulfur (S₈, C.P.), Carbon disulfide (CS₂, A.R.) and 200 proof ethanol (EtOH, A.R.) are purchased from Sinopharm Chemical Reagent Co., Ltd., which were used as received.

2.2 Preparation of I-HCSs@CT

The AAO templates were immersed in 0.2 M ethanol solution of FeCl₃·6H₂O for about 30 min, followed by drying. Then the AAO template were deposited PPy by vapor phase deposition process for 3 days (PPy@AAO). SiO₂ latex were prepared by the Stöber-Fink-Bohn method.²¹ The particle sizes were measured to be 64.1 ± 3.25 nm (Fig. S1). Subsequently, the PPy@AAO membrane was immersed in 10 mL of SiO₂ nanoparticles (NPs) in ethanol (~2 mg·mL⁻¹) for 3 days, followed by drying. The SiO₂@PPy@AAO templates were coated by PPy again, which lasted for 5 days. The

obtained samples were further carbonized to fabricate I-HCSs@CT (at 800 °C for 1.5 h). Finally, the samples were immersed into 3M NaOH and 10 % HF to remove AAO and SiO₂, respectively.

2.3 Preparation of CTs and H-HCSs@CT

The preparation methods were reported in our previous work.²²

2.4 Sulfur Impregnation

The S impregnation processes were implemented by the melting-diffusion method.¹⁸ The CT-based materials with a C:S (a weight ratio of 1:5) were first ball-milled for 2 h and then heated in a tube furnace at 160 °C for 12 h under N₂ atmosphere. The excess sulfur was washed by CS₂.

2.5 Characterization

Scanning electron microscopy (SEM) images were obtained with Quanta 400 FEG. Transmission electron microscope (TEM), scanning transmission electron microscope (STEM) imaging and energy dispersive X-Ray (EDX) mapping were performed on a FEI Tecani G2 F20 S-TWIN. X-ray photoelectron spectroscopy (XPS) measurements were performed using an ESCALAB 250 instrument (Thermo Electron) with Al Kα radiation. Element analysis (EA) was performed using Vario EL cube. The nitrogen sorptions of the samples were measured at 77 K using NOVA 2000 (Micromeritics ASAP 2020). The electrical resistivity was measured, using four-probe resistivity measurement system (SX1944).

2.6 Electrochemical measurements

The working electrodes were composed of 80 wt % of S-C composite, 10 wt % of acetylene black (conductive agent), and 10 wt % of polyvinylidene difluoride (PVDF) (binder). The S-C composite electrode (~3.5 mg cm⁻²) was loaded onto the aluminum foil and the thickness of electrode materials was ~30 micrometers. Lithium foil was used as reference electrode. The electrolyte (~0.06 ml) was 1 M bis(trifluoromethane) sulfonamide lithium salt (LiTFSI, Sigma Aldrich) dissolved in a mixed solvent of 1,3 dioxolane (DOL, Acros Organics) and 1,2 -dimethoxyethane (DME, Acros Organics) with a volume ratio of 1:1. The coin cells were assembled in an argon-filled glove-box. Electrochemical measurements were performed on a LAND-CT2001C test system. The coin cells were discharged (lithium insertion) and charged (lithium extraction) at 0.1 C (1 C = 1670 mA g⁻¹) in the fixed voltage range of 1.5 V to 3.0 V (vs. Li⁺/Li). Coulombic efficiency was defined as charge capacity / discharge capacity. High rates (0.5, 1, or 2 C) were also used and the first-cycle discharging was kept at 0.1 C. Nyquist plots were collected on a CHI660D electrochemical workstation for various electrodes from 100 kHz to 10 mHz.

3. Results and Discussion

3.1 Process and structures

In our previous work, hollow carbon spheres in carbonaceous

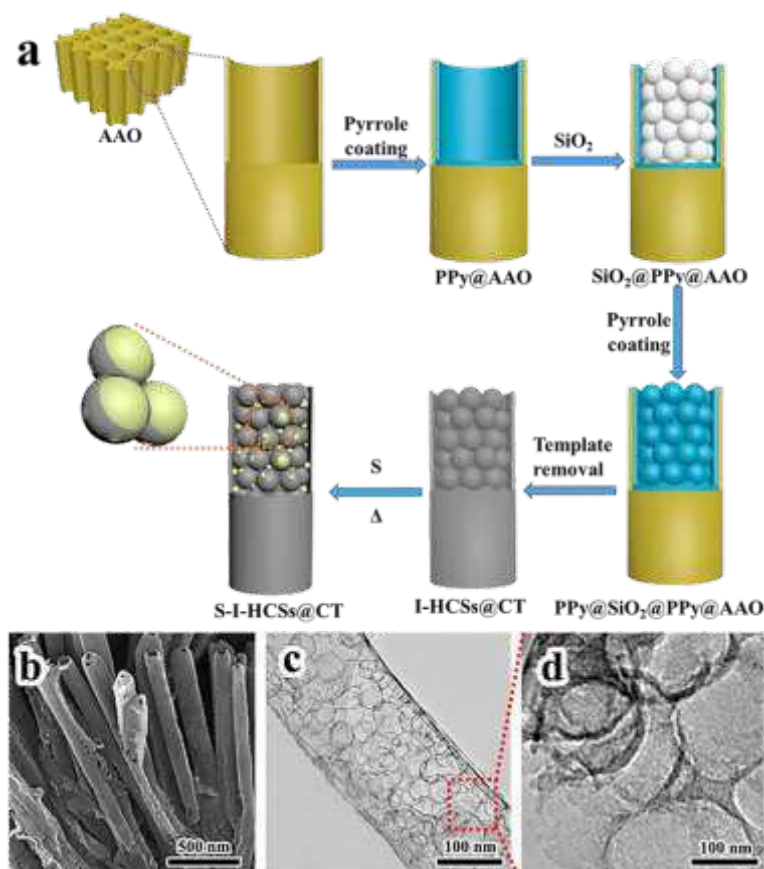


Fig. 1. a) Schematic illustrations of the production of S-I-HCSs@CT by confined assembly. In the enlarged view of S-I-HCSs@CT, sulfur not only fills the inner void space of HCSs, but also exists in the space between HCSs; b) SEM and c) TEM images showing I-HCSs@CT with smooth surface. HRTEM image d) showing few mesopores on the surface of I-HCSs@CT.

tube structure with holy surface (H-HCSs@CT) has been prepared, which is illustrated in Fig. S2.²² This novel spheres-in-tube structure with hierarchical pores and large specific surface area facilitates the transport and storage of the charges. However, holy surface of CT may be less efficient in inhibiting the dissolution of intermediate polysulfides. A new spheres-in-tube structure with intact CT was developed in this work, which is named as I-HCSs@CT. The preparation procedure of I-HCSs@CT is shown in Fig. 1a. According to the established packing schemes accessible by spheres within confined channels,²³ the diameter of the sphere (d_s) relative to the AAO channel diameter (d_c) determines the packing modes of spheres in the tube. The diameter of SiO₂ NPs was fixed as 64 nm (Fig. S2) in this study. Based on the ratio ($\alpha = d_c/d_s$), SiO₂@AAO templates with septuple-helice packing ($\alpha = 3.33$) were achieved, as shown in Fig. S3.

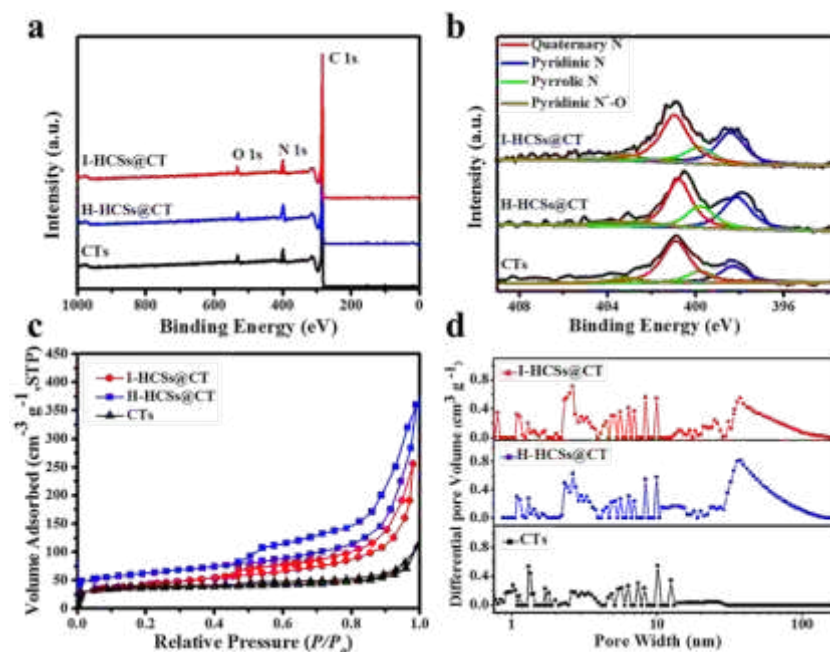
The obtained H-HCSs@CT and I-HCSs@CT were used to encapsulate sulfur materials at an elevated temperature of 160 °C to form S-H-HCSs@CT and S-I-HCSs@CT, respectively. In addition, S-CTs prepared by direct pyrolysis of PPy@AAO and template removal were used as a control sample, which is illustrated in Fig. S1.

The as-obtained three types of carbonized products (I-HCSs@CT, H-HCSs@CT and CTs) present different morphologies (Fig. 1a and Fig. S4a&b). Compared with bare CT structures (Fig. S4c&e), I-HCSs@CT and H-HCSs@CT possess ordered close-packed HCSs

encapsulated in CT (Fig. 1c and Fig. S4d). The meso/macropores can serve as channels for the penetration of sulfur, and hence increasing sulfur loading, which will be discussed further below. Notably, mesopores (~35-40nm) were generated uniformly on the surface of H-HCSs@CT (Fig. S4f), while smooth surface is observed for I-HCSs@CT (Fig. 1b), which can be further demonstrated by HRTEM images of I-HCSs@CT (Fig. 1d). According to these observations, we envisage that, our spheres-in-tube structure can perform well in enhancing the conductivity of sulfur electrode, inhibiting shuttle effect and buffering volume expansion of sulfur in cycling.

3.2 Chemical structures and compositions

The chemical compositions of all the three CTs-based samples were examined using X-ray photoelectron spectroscopy (XPS) (Fig. 2 and Fig. S5a) analysis. It can be seen from Fig. 2a, C1s, N1s and O1s are present in all the three samples. Nitrogen and oxygen have originated mainly from PPy and SiO₂@AAO templates, and are deemed to contribute to high capacitance as heteroatoms.²⁴ The high resolution C1s spectrum of CTs-based materials displayed six



View Article Online
DOI: 10.1039/C8TA05041D

Fig. 2. a) XPS survey spectra of I-HCSs@CT, H-HCSs@CT and CTs; b) High-resolution N1s XPS spectra of all the three samples; c) Nitrogen adsorption/desorption isotherms of all the three samples; d) Pore size distribution of all the three samples.

Table 1. Parameters of pore structures and elemental composition.

Samples	Textural properties				Chemical composition ^a (%)			
	S_{BET} ($\text{m}^2 \text{g}^{-1}$)	Pore Size (nm)	V_{total} ($\text{cm}^3 \text{g}^{-1}$)	V_{micro} ($\text{cm}^3 \text{g}^{-1}$)	C	N	H	O
I-HCSs@CT	287	7.54	0.61	0.14	86.36	9.41	0.31	3.91
H-HCSs@CT	318	9.23	0.78	0.09	87.25	8.74	0.52	3.39
CTs	184	5.12	0.29	0.06	86.43	6.98	1.72	4.87

a. Chemical composition was calculated by EA (Elemental analysis).

peaks, assigned to C=C, C-C, C-N, C-O, C=O and O=C-O (Fig. S5a),²⁵ The presence of these peaks revealed the abundance of oxygen-containing groups in the three samples, which would be beneficial for enhancing the adsorption ability of sulfur.¹⁶ The high resolution N1s spectra of the three samples were deconvoluted into four peaks: 398.5 ± 0.2 , 399.9 ± 0.1 , 401.1 ± 0.2 and 403.2 ± 0.8 eV (Fig. structure of CTs-based materials containing N and O functional groups is proposed in Fig. S5b).

The results of Elemental Analysis for these samples are given in Table 1. It can be seen that heterogeneity (N + O) of each sample reaches $\sim 11\%$, indicating that the nitrogen-enriched precursor and appropriate carbonization method used in this work can introduce rich nitrogen and oxygen-containing groups, favorable for the improvement of sulfur sorption as host materials.^{25, 27}

Nitrogen sorption experiments were employed to evaluate the porous structures and SSA of all samples, which are important properties for their uses as sulfur host materials. The results of Brunauer-Emmett-Teller (BET) surface area, pore volume, and average pore size are summarized in Table 1. The nitrogen

adsorption-desorption isotherms and corresponding pore size distribution (PSD) curves of all the three samples are shown in Fig. 2c&d. It can be seen from Fig. 2c that, all the nitrogen adsorption isotherms are of type-IV curves, and exhibit a steep rise at low relative pressure ($P/P_0 < 0.001$) reflecting the abundance of microporous structures, and a steep rise at high pressure ($P/P_0 = 1$) due to the presence of macropores formed by the removal of templates. The SSA of H-HCSs@CT ($318 \text{ m}^2 \text{g}^{-1}$) or I-HCSs@CT ($287 \text{ m}^2 \text{g}^{-1}$) is much larger than that of CTs ($184 \text{ m}^2 \text{g}^{-1}$) (Table 1), consistent with septuple helical packing of HCSs in the void space of the CT inner (Fig. 1c and Fig. S4d). The high SSA can play an

adsorption-desorption isotherms and corresponding pore size distribution (PSD) curves of all the three samples are shown in Fig. 2c&d. It can be seen from Fig. 2c that, all the nitrogen adsorption isotherms are of type-IV curves, and exhibit a steep rise at low relative pressure ($P/P_0 < 0.001$) reflecting the abundance of microporous structures, and a steep rise at high pressure ($P/P_0 = 1$) due to the presence of macropores formed by the removal of templates. The SSA of H-HCSs@CT ($318 \text{ m}^2 \text{g}^{-1}$) or I-HCSs@CT ($287 \text{ m}^2 \text{g}^{-1}$) is much larger than that of CTs ($184 \text{ m}^2 \text{g}^{-1}$) (Table 1), consistent with septuple helical packing of HCSs in the void space of the CT inner (Fig. 1c and Fig. S4d). The high SSA can play an

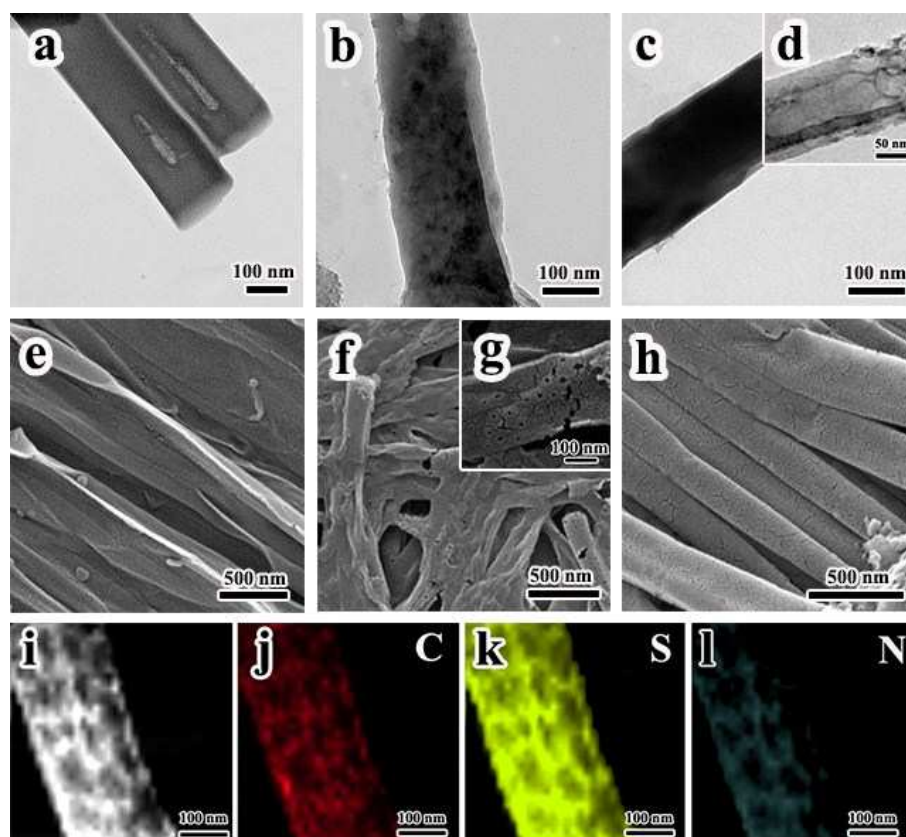
View Article Online
DOI: 10.1039/C8TA05041D

Fig. 3. TEM images of products: a) S-CTs, b) S-H-HCSs@CT, c)&d) S-I-HCSs@CT. SEM images of products: e) S-CTs, f)&g) S-H-HCSs@CT and h) S-I-HCSs@CT. i) STEM image, and j), k), l) EDX-mapping of the sulfur-embedded I-HCSs@CT: j) carbon, k) sulfur and l) nitrogen.

important role in increasing sulfur loading and inhibiting the shuttle effect of polysulfides. The porosity curves of the three samples all possessed peaks from 0.81 nm to 15 nm, which may result from the pyrolysis of PPy.^{25,27} In addition, I-HCS@CT and H-HCSs@CT owned wide distribution of meso/macropores from 20 nm to 100 nm, with the onset of the extremum at 38.1 nm, mainly attributed to the removal of SiO₂ templates. The pore volume with the size 38.1 nm of I-HCSs@CT is lower than that of H-HCS@CT, mainly due to the existence of fewer mesopores on the surface of I-HCSs@CT (Fig. 1b). The hierarchical porous structures count for the improved electrochemical performance, since the macropores can facilitate sulfur penetration, and the micropores and mesopores are beneficial for increasing the sulfur loading and electrical contact between sulfur and carbon host materials. Importantly, I-HCSs@CT can effectively block the contact of lithium polysulfides and electrolytes, thanks to its intact nature with fewer mesopores on the surface.

3.3 Lithium-sulfur electrochemistry performance

Owing to the high surface area and heteroatoms of I-HCSs@CT, the as-prepared carbon structure was used to prepare the sulfur-carbon composite nanomaterial. S-I-HCSs@CT, S-H-HCSs@CT and S-CTs were prepared by dipping samples into molten sulfur, where sulfur above the melting point is imbedded into the pores in the carbonaceous structure by capillary forces. Then, it solidifies and shrinks to form nanoscale sulfur component in the inner space (Fig. 1a and Fig. S1). Low-magnification SEM images of the final products

(Fig. S6) present the morphology with a large bundle of nanotubes for each sample. Furthermore, as shown in Fig. 3a-c&e&f&h, the S-I-HCSs@CT, S-H-HCSs@CT and S-CTs exhibit tube morphology without aggregation of the sulfur observed on the surfaces of CTs. Although it is hard to observe HCSs inside a CT due to the presence of sulfur in TEM images, some HCSs are visible in the tip section (Fig. 3d), where negligible amount of sulfur materials exists. In addition, some mesopores are shown on the surface of S-H-HCSs@CT in Fig. 3g, where sulfur failed to fill the pores. The wall of CT in S-I-HCSs@CT has a thickness of ~5 nm and its amorphous nature can

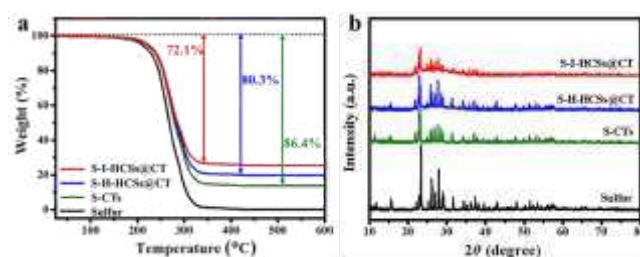


Fig. 4. a) TGA and b) XRD patterns of elemental sulfur (black), S-I-HCSs@CT (red), S-H-HCSs@CT (blue) and S-CTs (green).

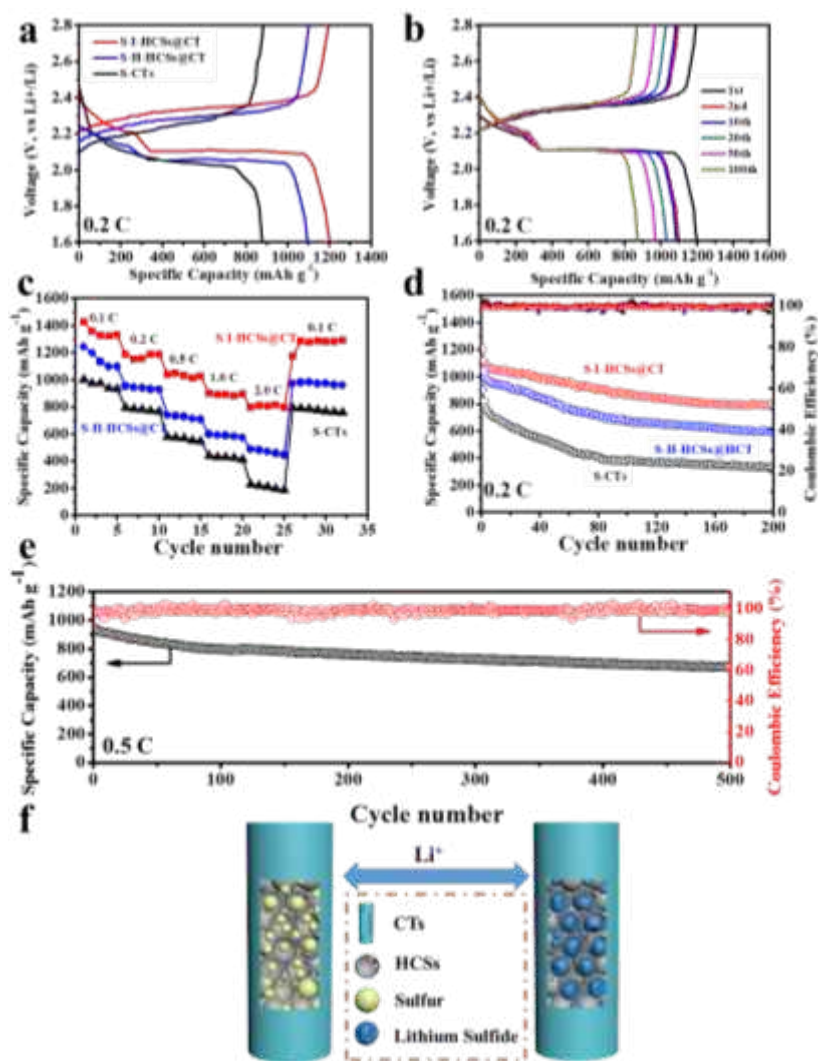


Fig. 5. Electrochemical performance of S-I-HCSs@CT, S-H-HCSs@CT and S-CTs electrodes (1 C = 1670 mA g⁻¹): a) First discharge/charge curves of the three samples at 0.2 C; b) Discharge/charge voltage profiles of S-I-HCSs@CT at 0.2 C; c) Rate performance of the three samples at stepwise current rates; d) Cycling performance of S-I-HCSs@CT, S-H-HCSs@CT and S-CTs at 0.2 C; e) Cycling performance of S-I-HCSs@CT at 0.5 C for 500 cycles; f) Schematic diagram of the mechanism for the reversible electrochemical reaction of S-I-HCSs@CT.

benefit the lithium insertion and extraction, contributing to good Li-ion accessibility to the filled sulfur and HCSs.^{30,31} Moreover, scanning tunneling electron microscopy (STEM) image and EDX-mapping analysis of S-I-HCSs@CT reveal that the sulfur component fills the inner void space of HCSs and the space between HCSs rather than being adhered on the surface of CT (Fig. 3i-l).

It is worthy note that, the incorporation of HCSs into CT leads to the close contact between HCSs and sulfur materials, thus further increasing their electrical conductivity and mechanical stability during cycling with lithium ions.

Thermogravimetric analysis (TGA) and X-ray diffraction (XRD) were employed to investigate the composition and crystallinity of the sulfur-carbon nanocomposites. Fig. 4a shows the TGA curves of pure sulfur and three types of sulfur-carbon nanocomposites. These samples display continuous weight loss from 180 to 370 °C in a nitrogen environment. The S-I-HCSs@CT presents a weight loss of ≈ 72%, while the S-H-HCSs@CT exhibits ≈ 80% of weight loss and S-

CTs shows ≈ 86% of weight loss. Therefore, CTs possess the largest sulfur content due to the largest cavity. S-H-HCSs@CT shows higher weight loss than S-I-HCSs@CT, because of abundant ordered mesopores on the surface of H-HCSs@CT, which provide pathways for the diffusion of sulfur. In general, all the three samples show high sulfur loading owing to the higher surface area with small pores and heteroatoms in the samples.^{19,20} XRD patterns of the pure sulfur and the carbon-sulfur composites are given in Fig. 4b. For all the three samples, the diffraction peaks corresponding to orthorhombic sulfur (JCPDS 08-2047) indicate the existence of sulfur. On the other hand, the S-I-HCSs@CT displays lowest intensity of sulfur diffraction peaks because the sulfur component is well confined in the carbon nanostructure and functional groups on the carbon surface prevent sulfur growing into crystalline particles.³²

Additionally, the S-I-HCSs@CT exhibit a significant decrease in BET surface area (from 287 to 18 m² g⁻¹) and smaller pores upon the introduction of sulfur, as shown in Fig. S7.

To assess the applicability of the S-I-HCSs@CT as a cathode material for Li-S batteries, the electrochemical performances were tested with coin cells. Fig. 5a shows the initial discharge and charge profiles of S-I-HCSs@CT, S-H-HCSs@CT and S-CTs within a voltage window of 1.6-2.8 V at 0.2 C. The three sulfur-carbon composites all exhibit two discharge plateaus at ~2.3 and 2.0 V, which can be ascribed to the formation of long-chain polysulfides (Li₂S_x, 4 ≤ x ≤ 8) and insoluble Li₂S. The charge plateau from ~2.2 to 2.5 V corresponds to the formation of Li₂S_x (4 ≤ x ≤ 8) and final S₈.^{33,34} Strikingly, compared with the discharge capacity for S-CTs (867 mAh g⁻¹) and S-H-HCSs@CT (1104 mAh g⁻¹), S-I-HCSs@CT exhibits a substantially higher discharge capacity of 1206 mAh g⁻¹, suggesting a high utilization rate of sulfur, which relies on the merits of orderly packed HCSs and intact CT wall. These electrically conductive HCSs have intimate contact with sulfur cathode, thus offering good electrical contact between sulfur cathodes and the current collector. As a result, almost all sulfur cathodes can exhibit electrochemical activity during the first-cycle cycling. More importantly, the capacity of S-I-HCSs@CT is 1113 mAh g⁻¹ in the second cycle and much better capacity retention was demonstrated (Fig. 5b and Fig. S8). In addition, the good overlap of the discharge plateaus during the cycling test also suggested the better stability and reversibility of the electrode than those of S-H-HCSs@CT and S-CTs. Cyclic voltammetry (CV) curves of Li-S cells with S-I-HCSs@CT as a cathode are shown in Fig. S9. The variation in the anodic peaks between the first and second cycles can be attributed to the rearrangement of active sulfur from its original positions to more energetically stable sites. No significant changes were detected for either of the anodic/cathodic peaks in the subsequent three cycles, indicating a high electrochemical stability of S-I-HCSs@CT.

Fig. 5c compares high-rate performance of S-I-HCSs@CT, S-H-HCSs@CT and S-CTs. They all showed high initial specific discharge capacities at a 0.1 C rate: 1426 mAh g⁻¹ for S-I-HCSs@CT, 1245 mAh g⁻¹ for S-H-HCSs@CT, and 1006 mAh g⁻¹ for S-CTs. However, except for the S-I-HCSs@CT, the capacity of the electrodes significantly decreases with increasing current rate. On the other hand, S-I-HCSs@CT exhibits a reasonable capacity of 814 mAh g⁻¹ at 2 C rate. Fig. 5d shows the cycling performance of S-I-HCSs@CT, S-H-HCSs@CT and S-CTs at 0.2 C. The discharge capacity of S-CTs is retained at 329 mAh g⁻¹ after 200 cycles. In contrast, S-H-HCSs@CT exhibits higher discharge capacity of 673 mAh g⁻¹ after 200 cycles. More significantly, S-I-HCSs@CT presents the highest discharge capacity of 864 mAh g⁻¹ after 200 cycles. The average capacity fading rate for S-I-HCSs@CT is calculated to be 0.13 % per cycle, smaller than 0.21 % for S-H-HCSs@CT and 0.34 % for S-CTs. Therefore, the S-I-HCSs@CT cathode demonstrates the best cycling performances. Moreover, the S-I-HCSs@CT electrode displays a much higher Coulombic efficiency than the other two electrode materials, indicating that polysulfide dissolution into the organic electrolyte was effectively mitigated in the former, which was further evidenced through visual observation (Fig. S10&11).

In addition, the cycling performance of S-I-HCSs@CT is also determined in a higher current rate (0.5 C) for 500 cycles (Fig. 5e).

The discharge capacity of S-I-HCSs@CT after 500 cycles is retained at 746 mAh g⁻¹ with high Coulombic efficiency that is 78.1% capacity retention compared with the initial discharge capacity, demonstrating outstanding cycling stability. In addition, the detectable capacity of the sample at 0.5 C fades faster compared with that at 0.2 C. This should mainly result from the limitation of the electrical conductivity of the sulfur/carbon composite, which cannot satisfy the requirement for such a faster discharge and charge during repetitive cycling.^{17,35} The performance of Li-S batteries with different sulfur host materials are summarized in Table S1, which corroborates that S-I-HCSs@CT own superior cycling performance.

Nyquist plots of S-I-HCSs@CT, S-H-HCSs@CT and S-CTs after the third cycle are shown in Fig. S12a. Compared with S-CTs, S-I-HCSs@CT or S-H-HCSs@CT has a smaller semicircle, indicating a lower charge transfer resistance (*R*_{ct}) at the electrode interface. On the basis of the equivalent circuit,³⁶ the value of *R*_{ct} in S-I-HCSs@CT or S-H-HCSs@CT is 29.6 Ω or 31.4 Ω, respectively, substantially smaller than that of S-CTs (171.8 Ω). The low *R*_{ct} is considered to arise from the intimate contact of HCSs and sulfur, which remarkably increases the electrical contact of the insulating sulfur cathode. In addition, the stability of the S-I-HCSs@CT electrode is also evidenced by the EIS data before and after 500 cycles at 0.5 C rate (Fig. S12b). The charge-transfer resistance (*R*_{ct}) is calculated to be 35.8 Ω after cycling, which is close to the value (29.6 Ω) before cycling, suggesting excellent stability and a high electrical conductivity of S-I-HCSs@CT. Moreover, the electrical resistivities of the three samples were measured using a four-probe resistivity measurement system. The S-I-HCSs@CT (483 Ω cm) has lower resistivity than that of S-H-HCSs@CT (529 Ω cm) or S-CTs (673 Ω cm) at 25 °C (Fig. S13), which corroborates the good electrochemistry activity of S-I-HCSs@CT.

Based on the above discussions, we ascribe the excellent electrochemical performance of S-I-HCSs@CT, including large reversible capacity and good high-rate cycling stability, to the following features associated with this sphere-in-tube carbonaceous/sulfur nanostructure (as illustrated in Fig. 5f and Fig. S14&15): (1) The presence of HCSs packed closely with sulfur inside a large CT provide huge cavities or inter pores for sulfur impregnation, and increases the electrical conductivity of sulfur. Also, the interior void space can buffer the volume change to some extent, which is evidenced by the change of electrode thickness in the three samples (Fig. S16).³⁷ (2) The intact wall of CT can serve as a confinement layer to constrain sulfur strictly in the inner void space of HCSs, which hinders the direct contact of lithium polysulfides with electrolytes and hence prevents the dissolution of sulfur in the electrolyte, eventually improving the utilization rate of sulfur.^{38,39} (3) The HCSs framework can play a role of electric connections, even if sulfur materials are detached from the interior surface of HCSs and the wall of CT, which boost the improvement of cycling stability, because the detachment of sulfur materials from carbon surface and the subsequent loss of their electrochemical activity have been previously demonstrated to be a crucial cause of

poor cycling stability for sulfur cathode.⁴⁰ (4) The overall spheres-in-tube structure offers a shortened diffusion pathway for rapid transport of ions and electrons, which is very important for enhancing the high utilization rate of sulfur especially at a large discharge and charge current.

4. Conclusions

In summary, a sphere-in-tube carbon structure with HCSs confined in an intact CT has been developed as an effective sulfur host with a high sulfur loading of 72.1 wt % in Li-S batteries. In our rationally design nanoarchitecture, the intimate contact of HCSs and sulfur cathodes contributes to increased electrical conductivity and improved structure stability. The intact CT wall acts as a barrier for effectively inhibiting the dissolution of lithium sulfur, and the interior cavity can mitigate the volume change. The overall spheres-in-tube facilitates the rapid transport of ions and electrons. Benefiting from the synergy of these merits, S-I-HCSs@CT exhibits a large reversible capacity of 1206 mAh g⁻¹ at 0.2 C and 814 mAh g⁻¹ at 2.0 C with excellent high-rate performance. In addition, a high specific capacity of 746 mAh g⁻¹ at 0.5 C can be retained after 500 cycles, which shows excellent cycling stability of S-I-HCSs@CT electrode. Taken together, these results demonstrate the great potential of sphere-in-tube nanostructure to be exploited as an electrode for Li-S batteries, and provide valuable insights on the rational design of hybrid carbon nanostructure suitable for high-performance Li-S batteries.

Conflicts of interest

There are no conflicts to declare

Acknowledgements

The financial support from the National Natural Science Foundation of China (No. 21104050, 11604045), China Postdoctoral Science Foundation (2013M541715, 2014T70541), a Project Funded by the Priority Academic Program Development of Jiangsu Higher Education Institutions (PAPD), the fund (2017002) from Key Laboratory of Advanced Textile Materials and Manufacturing Technology (Zhejiang Sci-Tech University), Ministry of Education, the Fundamental Research Funds for the Central Universities, Shanghai Science and Technology Commission 16PJ1400100, 17ZR1440000, and 17JC400700 are gratefully acknowledged.

References

- 1 A. Burke, *J. Power Sources*, 2000, **91**, 37-50.
- 2 P. G. Bruce, S. A. Freunberger, L. J. Hardwick and J. M. Tarascon, *Nat. Mater.*, 2012, **11**, 19-29.
- 3 X. L. Ji and L. F. Nazar, *J. Mater. Chem.*, 2010, **20**, 9821-9826.
- 4 Y. X. Yin, S. Xin, Y. G. Guo and L. J. Wan, *Angew. Chem. Int. Ed.*, 2013, **52**, 13186-13200.
- 5 Y. K. Wang, R. F. Zhang, Y. C. Pang, X. Chen, J. X. Lang, J. J. Xu, C. H. Xiao, H. L. Li, K. Xi and S. J. Ding, *Energy Storage Mater.*, 2019, **16**, 228-235.
- 6 Y. Yang, G. Zheng and Y. Cui, *Chem. Soc. Rev.*, 2013, **42**, 3018-3032.
- 7 Y. S. Su and A. Manthiram, *Nat. Commun.*, 2012, **3**, 1166.
- 8 Z. Lin, Z. Liu, W. Fu, N. J. Dudney and C. Liang, *Angew. Chem. Int. Ed.*, 2013, **52**, 7460-7463.
- 9 X. Liang, Z. Y. Wen, Y. Liu, M. F. Wu, J. Jin, H. Zhang and X. W. Wu, *J. Power Sources*, 2011, **196**, 9839-9843.
- 10 Y. H. Cui, Q. Zhang, J. W. Wu, X. Liang, A. P. Baker, D. Y. Qu, H. Zhang, H. Y. Zhang and X. H. Zhang, *J. Power Sources*, 2018, **378**, 40-47.
- 11 Y. K. Wang, S. J. Wang, T. T. Zhao, Y. Chen, Z. T. Li, W. T. Wu and M. B. Wu, *Chem. Eng. J.*, 2016, **306**, 336-343.
- 12 H. J. Peng, J. Q. Huang, M. Q. Zhao, Q. Zhang, X. B. Cheng, X. Y. Liu, W. Z. Qian and F. Wei, *Adv. Funct. Mater.*, 2014, **24**, 2772-2781.
- 13 F. Y. Jin, S. Xiao, L. J. Lu and Y. Wang, *Nano Lett.*, 2015, **16**, 440-447.
- 14 Z. J. Fan, J. Yan, L. J. Zhi, Q. Zhang, T. Wei, J. Feng, M. L. Zhang, W. Z. Qian and F. Wei, *Adv. Mater.*, 2010, **22**, 3723-3728.
- 15 A. Afzal, F. A. Abulhaiwi, A. Habib, M. Awais, S. B. Waje and M. A. Atieh, *J. Power Sources*, 2017, **352**, 174-186.
- 16 Z. Li, J. T. Zhang and X. W. D. Lou, *Angew. Chem. Int. Ed.*, 2015, **54**, 12886-12890.
- 17 Y. Zhou, C. G. Zhou, Q. Y. Li, C. J. Yan, B. Han, K. S. Xia, Q. Gao and J. P. Wu, *Adv. Mater.*, 2015, **27**, 3774-3781.
- 18 Y. Yang, G. H. Yu, J. J. Cha, H. Wu, M. Vosgueritchian, Y. Yao, Z. A. Bao and Y. Cui, *ACS Nano*, 2011, **5**, 9187-9193.
- 19 W. Y. Li, Q. F. Zhang, G. Y. Zheng, Z. W. Seh, H. B. Yao and Y. Cui, *Nano Lett.*, 2013, **13**, 5534-5540.
- 20 G. C. Li, G. R. Li, S. H. Ye and X. P. Gao, *Adv. Energy Mater.* 2012, **2**, 1238-1245.
- 21 W. Stöber, A. Fink and E. Bohn, *J. Colloid Inter. Sci.*, 1968, **26**, 62-69.
- 22 Z. Chen, S. J. Ye, S. D. Evans, Y. H. Ge, Z. F. Zhu, Y. F. Tu and X. M. Yang, *Small*, 2018, **14**, 1704015.
- 23 R. O. Erickson, *Science*, 1973, **181**, 705-716.
- 24 Z. Chen, R. Cao, Y. H. Ge, Y. F. Tu, Y. Xia and X. M. Yang, *J. Power Sources*, 2017, **363**, 356-364.
- 25 C. Zhang, W. Lv, Y. Tao and Q. H. Yang, *Energy Environ. Sci.*, 2015, **8**, 1390-1403.
- 26 Z. X. Xu, X. D. Zhuang, C. Q. Yang, J. Cao, Z. Q. Yao, Y. P. Tang, J. Z. Jiang, D. Q. Wu and X. L. Feng, *Adv. Mater.*, 2016, **28**, 1981-1987.
- 27 C. X. Guo, N. Li, L. L. Ji, Y. W. Li, X. M. Yang, Y. Lu and Y. F. Tu, *J. Power Sources*, 2014, **247**, 660-666.
- 28 J.-S. Lee, W.-Y. Kim, J.-S. Jang and A. Manthiram, *Adv. Energy Mater.*, 2016, 1601943.
- 29 G. Y. Zheng, Y. Yang, J. J. Cha, S. S. Hong and Y. Cui, *Nano Lett.*, 2011, **11**, 4462-4467.
- 30 C. F. Zhang, H. B. Wu, C. Z. Yuan, Z. P. Guo and X. W. D. Lou, *Angew. Chem. Int. Ed.*, 2012, **51**, 9592-9595.
- 31 W. D. Zhou, C. M. Wang, Q. L. Zhang, H. D. Abruña, Y. He, J. W. Wang, S. X. Mao and X. C. Xiao, *Adv. Energy Mater.*, 2015, 1401752.
- 32 C. Zu and A. Manthiram, *Adv. Energy Mater.*, 2013, **3**, 1008-1012.

- 33 Y. C. Qiu, W. F. Li, W. Zhao, G. Z. Li, Y. Hou, M. N. Liu, L. S. Zhou, F. M. Ye, H. F. Li, Z. H. Wei, S. H. Yang, W. H. Duan, Y. F. Ye, J. H. Guo and Y. G. Zhang, *Nano Lett.*, 2014, **14**, 4821-4827.
- 34 S. Xiao, S. H. Liu, J. Q. Zhang and Y. Wang, *J. Power Sources*, 2015, **293**, 119-126.
- 35 Y. Zhao, W. L. Wu, J. X. Li, Z. C. Xu and L. H. Guan, *Adv. Mater.*, 2014, **26**, 5113-5118.
- 36 F. Y. Jin and Y. Wang, *J. Mater. Chem. A*, 2015, **3**, 14741-14749.
- 37 W. D. Zhou, Y. C. Yu, H. Chen, F. J. DiSalvo and H. D. Abruna, *J. Am. Chem. Soc.*, 2013, **135**, 16736-16743.
- 38 G. Q. Ma, Z. Y. Wen, J. Jin, Y. Lu, X. W. Wu, M. F. Wu and C. H. Chen, *J. Mater. Chem. A*, 2014, **2**, 10350-10354.
- 39 W. Y. Li, G. Y. Zheng, Y. Yang, Z. W. Seh, N. Liu and Y. Cui, *Proc. Natl. Acad. Sci. U.S.A.*, 2013, **110**, 7148-7153.
- 40 C. Wang, W. Wan, J. T. Chen, H. H. Zhou, X. X. Zhang, L. X. Yuan and Y. H. Huang, *J. Mater. Chem. A*, 2013, **1**, 1716-1723.

View Article Online
DOI: 10.1039/C8TA05041D

A sphere-in-tube carbonaceous nanostructure has been prepared as an effective sulfur host, exhibiting large reversible capacity and good cycling stability.

